4. Discussion

4.1 Preparation of oxalato complexes

$K_3[Cr(C_2O_4)_3]\cdot 3H_2O$ and $K_3[Al(C_2O_4)_3]\cdot 3H_2O$ complexes were prepared according to the literature procedures (Booth, 1939). Chromium oxalate is dark bluish green and aluminium oxalate is colorless crystals. Both complexes are nearly isomorphous and have been reported as belong to the same space group $P2_1/c$ with four molecules per unit cell (Taylor, 1978). Solubilities of both starting complexes and the products were studied with various solvents. The solubility results are given in Table 2 (Chapter 3). All the complexes were readily soluble in water, slightly soluble in less polar solvents and insoluble in non-polar solvents.

4.2 Products characterizations

4.2.1 Titration technique

$K_3[Al(C_2O_4)_3].3H_2O$ contains potassium, as the counter ion, and the complex anion, $[Al(C_2O_4)_3]^{3-}$, with three water molecules. The purity of the complex can be determined by analyzing its constituents (potassium, aluminium, and oxalate) and comparing the experimental values with the calculated values. The relative percentages of all the constituents can be determined in order to comfirm the above stoichiometry of the complex. In this experiment the oxalate content of the complex was determined. The complex was decomposed by addition of excess sulfuric acid.

$$K_3[Al(C_2O_4)_3].3H_2O + 3H_2SO_4 \rightarrow 3H_2C_2O_4 + 3K^+ + Al^{3+} + 3SO_4^{2-} + 3H_2O$$

The oxalic acid thus released into the solution could be determined by titration with a standard solution of $KMnO_4$ which acted as an oxidant. The oxidation state of manganese in $KMnO_4$ was Mn^{7+} which was reduced to Mn^{2+} in hot acid solution (or

else it was converted to MnO_2) by accepting five electrons from the oxalate ion which in turn acted as a reductant and was oxidised to CO_2 as shown in the reaction equations:

$$MnO_{4\,(aq)}^{-} + 8H^{+}_{(aq)} + 5e^- \longrightarrow Mn^{2+}_{(aq)} + 4H_2O_{(l)}$$

$$C_2O_4^{2-}{}_{(aq)} \longrightarrow 2CO_{2(g)} + 2e^-$$

The MnO_4^- half-reaction must be multipled by 2, and the $C_2O_4^{2-}$ half-reaction must be multiplied by 5 so that the same number of electrons(10) appears on both sides of the equations:

$$10e^- + 16H^{+}_{(aq)} + 2\,MnO_{4\,(aq)}^{-} \longrightarrow 2Mn^{2+}_{(aq)} + 8H_2O_{(l)}$$

$$5C_2O_4^{2-}{}_{(aq)} \longrightarrow 10CO_{2(g)} + 10e^-$$

The balanced equation is the sum of the balanced half-reactions. Note that the electrons on the reactant and product sides of the equation cancel each other.

$$16H^{+}_{(aq)} + 2\,MnO_{4\,(aq)}^{-} + 5C_2O_4^{2-}{}_{(aq)} \longrightarrow 2Mn^{+}_{(aq)} + 8H_2O_{(l)} + 10CO_{2(g)}$$

This method was utilized to indicate the percentage of oxalate group in complexes. The accepted experimental results must be close to the calculated data. In practice, the experimental data are usually slightly different from the calculated data because of the impurity, the moisture, and how sensitive the samples to air. These affect the higher or lower quantitative values of the results. The experimental and calculated data are compared in Table 1(Chapter 3). The percentage of oxalate group

in $K_3[Cr(C_2O_4)_3].3H_2O$ could not be determined due to mixed color at the end point. (Interference from the yellow color of Cr^{3+} ion at the end point.)

4.2.2 Elemental analysis

The percentages of K, Na, Cr, and Al in oxalato complexes by ICP-AES are listed in Table 2. Results of $K_3[Al(C_2O_4)_3].3H_2O$ and $K_3[Cr(C_2O_4)_3].3H_2O$ are close to the calculated values. In $K_3[Al(C_2O_4)_3].3H_2O$ it was found to contain 24.34% K (25.37%), 4.78% Al (5.84%) and in $K_3[Cr(C_2O_4)_3].3H_2O$ was 24.16% K (24.07%), 10.24% Cr (10.67%). The percentage values from the RedRhombo are similar to those obtained from x-ray data, these were 25.91% K (25.99%), 0.16% Na (0.00), 0.34% Cr (0.33), and 4.80% Al (5.51%). The RedCubic was found to contain 1.33% K, 8.99% Na, 0.51% Cr, and 4.56% Al whereas, the Blue contained 23.90% K, 0.00% Na, 0.59% Cr, and 4.52% Al. These values correspond to results from SEM/EDX technique which showed that they had similar compositions. The difference was in the content of Na and K. The RedCubic contains both Na and K while the RedRhombo and the Blue contain only K.

4.2.3 X-ray Powder Diffraction Patterns

The x-ray powder diffraction patterns of $K_3[Cr(C_2O_4)_3].3H_2O$ and $K_3[Al(C_2O_4)_3].3H_2O$ are identical to file 38-1446 of standard reference file with space group $P2_1/c$. In addition, the XRD pattern of the Blue is similar to $K_3[Cr(C_2O_4)_3].3H_2O$. The XRD pattern of the Redcubic from powder technique was similar to single crystal technique. But the space group could not be identified because the structure could not be solved. While the Redrhombo could be assigned to rhombohedral crystal system with $R\bar{3}$ space group.

4.2.4 X-ray single crystal data of $K_{18}\{K[Al_{0.97}Cr_{0.03}(C_2O_4)_3]_6\}Cl.18H_2O$, (RedRhombo)

The crystal structure of $K_3[Al(C_2O_4)_3].3H_2O$ consists of discrete $Al(C_2O_4)_3^{3-}$ anions, K^+ cations, and water molecules. Six oxygen atoms from water molecules and oxalate anions surround each of the K^+ atoms at distance varying from 2.306(1) to 2.995(7) Å. The structure of the tris(bidentate) $Al(C_2O_4)_3^{3-}$ complex shows a distorted octahedral coordination with angles O-Al-O between 83.1(2)° and 169.7(2)°, and Al-O distances varying between 1.876(3) and 1.913(4) Å (Talyor D., 1978). Similarly, the single crystal of $K_3[Cr(C_2O_4)_3].3H_2O$ consists of discrete $Cr(C_2O_4)_3^{3-}$ anions, K^+ cations and water molecules. Six oxygen atoms from water molecules and oxalate anions surround each of the K^+ atoms at distance varying from 2.349(7) to 3.008(5) Å. The structure of the tris(bidentate) $Cr(C_2O_4)_3^{3-}$ complex shows a distorted octahedral coordination with angles O-Cr-O between 81.8(1) ° and 171.0(1)°, and Cr-O distances varying between 1.955(2) and 1.985(2) Å (Talyor D., 1978).

In the $K_3[Cr(C_2O_4)_3].3H_2O$ complex, however, the two C-O bonds coordinated to the metal are lengthened (1.39 Å) and the two C=O bonds free from coordination are shortened (1.17 Å). Also, the C-C distance in the free ion is 1.56 Å (Fujita et al., 1962) and that in the complex is 1.25 Å. This C-C distance reduces to 1.551(6) Å in the $K_{18}\{K[Al_{0.97}Cr_{0.03}(C_2O_4)_3]_6\}Cl.18H_2O$ (RedRhombo). In the free ion, x-ray analysis indicates that four C-O bonds are equivalent, the distances being 1.27 Å (Fujita et al., 1962). The C-O distances in the ring varying between 1.275(5) to 1.293(5) Å whereas the free C=O distances varying between 1.212(5) and 1.225(5) Å and coordinated C-O distances with inner K are 1.231(5) Å in $K_{18}\{K[Al_{0.97}Cr_{0.03}(C_2O_4)_3]_6\}Cl.18H_2O$ (RedRhombo) complex.

The single crystal of $K_{18}\{K[Al_{0.97}Cr_{0.03}(C_2O_4)_3]_6\}Cl.18H_2O$ (RedRhombo) complex was grown in aqueous solution by slow solvent evaporation at room temperature. The coordination sphere around potassium, chromium, and aluminium are

distorted octahedron. The average bond angles of atoms in *cis* position of K(1) center, O(14)-K(1)-O(14) are in the range 84.3-95.7°, slightly deviating from the ideal octahedron (90°). Besides, the rhombohedral angles around Al(III) and Cr(III) are in the range 84.0-97.5° against 90° in ideal octahedron. The average bond angles of atoms in *trans* position of Al(III) and Cr(III) centers, O-Al-O and O-Cr-O, are in the range 171.4-172.8°. The K-O coordination distances are in the range 2.399(3) to 2.400 (3) Å. They are distances in $[K(H_2O)Cr(C_2O_4)_2(bpym)]$ which vary from 2.726(2) to 3.025(2) Å (Bérézovsky, et al., 1999). In addition, the K-O distances in [cis-Cr(III) $(C_2O_4)_2(DMSO)_2K(DMSO)_2]_n$ are 2.819(3) Å with the oxalate acts as a bidentate ligand (Öhrstrom et al., 2000). However, in $K_{18}\{K[Al_{0.97}Cr_{0.03}(C_2O_4)_3]_6\}Cl.18H_2O$ (RedRhombo) the oxalates that bond to K act as monodentate ligands. The average bonds distances of Al-O and Cr-O in this complex are 1.90 Å attributed to covalent bond which are shorter than the K(1)-O(14) distance.

4.2.5 UV- Visible absorption spectrometry

UV-Vis absorption spectra were determined both in solution and solid state: solution by using SPECORD S100 (Analytik Jena GmbH, 200-800 nm) and solid state by using UV-2401 (Shimadzu, 240-800 nm). The absorption spectra of all oxalato complexes in water were recorded in 200-800 nm and shown in Figure 6 (Chapter 3). The aqueous solution of all products were green. The spectra of product complexes were very similar to that of $[Cr(C_2O_4)_3]^{3-}$ ion which showed three bands at 420, 572, and 698 nm (Krishnamurty, 1960). The color is caused by $[Cr(C_2O_4)_3]^{3-}$ ions. The electronic spectra of all products in aqueous solutions show peaks at 420 and 572 nm similar to $[Cr(C_2O_4)_3]^{3-}$ (420 and 571 nm) (Bérézovsky et al., 1999). However, they were slightly different in solid state due to the slightly different environment in crystal exerting slightly different force field to the $[Cr(C_2O_4)_3]^{3-}$ complex, therefore, causing some minor shifts to these maxima which were summarized in Table 9 (Chapter 3).

The strong absorption at about 300 nm are generally assigned to ligand-centered $\pi \rightarrow \pi^*$ transition, most likely due to transition of the π electrons of the C=O group (Graddon D. P., 1956). In this work, oxalate ligand exhibits one intense band at 298 nm which can be assigned to the $\pi \rightarrow \pi^*$ electronic transitions in Figure 6 (Chapter 3). The two less intense bands (420 and 572 nm) in the visible spectra can be assigned to d-d transition at the Cr^{3+} center. The band at 298 nm has very high intensity due to its allowed $\pi \rightarrow \pi^*$ transition nature while bands at 420 and 572 nm are much weaker due to its being the d-d transition in nature. Theoretically, the d-d transition should be La Porte forbidden but became allowed due to the vibronic coupling so its intensity is much weaker.

The $[Cr(C_2O_4)_3]^{3-}$ is Cr^{III}, d^3, which in an octahedral complex has each t_{2g} level singly occupied, giving a sort of half – filled shell stability shown in Figure 34. The observed spectral transitions (cm^{-1}) for $[Cr(C_2O_4)_3]^{3-}$ complex are ν_1 (17,500 cm^{-1} or 571 nm), ν_2 (24,000 cm^{-1} or 417 nm), and ν_3 (38,100 cm^{-1} or 263 nm) as summarized in Table 14 and shown in Figure 35a (but ν_3 is not experimentally observed because it is masked by the charge transfer spectrum (Huheey et al., 1993)). From the more detailed diagram in Figure 35b the lowest energy electronic transitions would be expected to be from the $^4A_2$ ground state to the $^4T_2$(570 nm) and $^4T_1$(420 nm) excited states (spin allowed) and to the ^2E, $^2T_1$, $^2T_2$(697 nm) excited states (spin forbidden) (Yager et al., 1979).

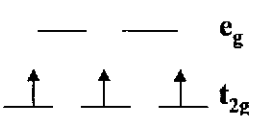

Figure 34 Orbital energy level diagram of Cr^{3+} (d^3) configuration in octahedral.

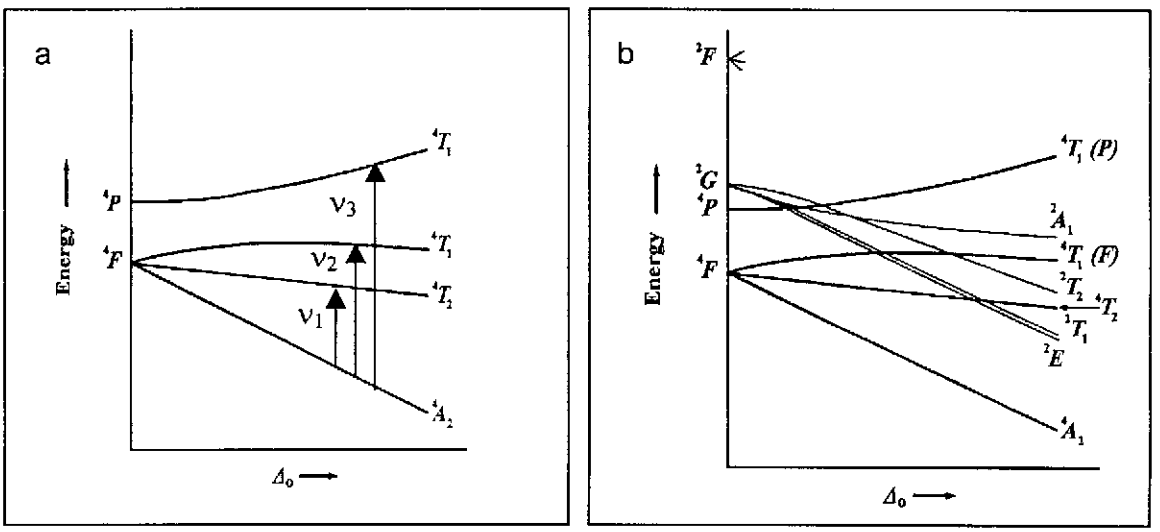

Figure 35 Partial energy-level diagram for a $Cr^{3+}(d^3)$ ion (a) and full energy-level diagram for a $Cr^{3+}(d^3)$ ion (b) in an octahedral field. (Cotton and Wilkinson, 1972)

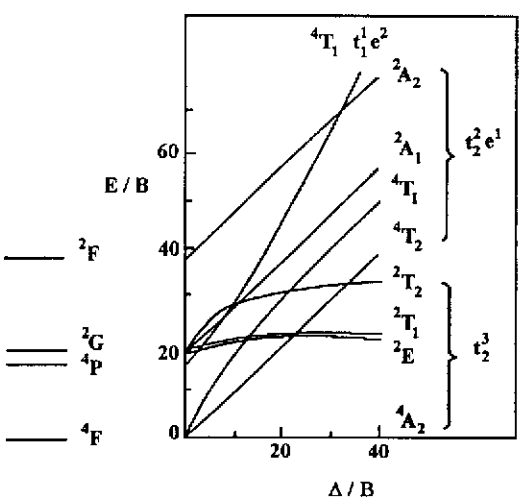

Figure 36 Tanabe-Sugano diagram for d^3 in octahedral field. The lower energy free-ion terms are shown on the left, and the diagram shows how the states evolve as a function of the CF splitting Δ. All energies are expressed in terms of the Racah *B* parameter; a fixed ratio *C/B* = 4.5 is assumed, and spin-orbit coupling neglected (Cox P. A., 1992).

The transition of Cr^{3+} has 3 bands as ν_1, ν_2, and ν_3 but ν_3 is not experimentally observed because it is close to the limit of instrument and also masked by the charge transfer spectrum (Huheey et al., 1993). Therefore, only ν_1 and ν_2 are observable and appear in the visible region. The spectrum of $[Cr(C_2O_4)_3]^{3-}$ is shown in Figure 6 (Chapter 3) and the data are summarized in Table 14. The bands ν_1 and ν_2 appear at 571 and 417 nm, respectively. The valley between ν_1 and ν_2 centers around 500 nm which corresponds to the green color. Therefore, the solution containing $[Cr(C_2O_4)_3]^{3-}$ ion, in this case, is green. Since the field strength of $C_2O_4^{2-}$ ligand is nearly equal that of H_2O, the ν_1, ν_2, and ν_3 of both ligands are given, for the sake of comparison, in Table 14.

Table 14 Calculated spectral transitions for $[Cr(C_2O_4)_3]^{3-}$ and $[Cr(H_2O)_6]^{3+}$ complex in aqueous solution.

ν	Transition band	$[Cr(C_2O_4)_3]^{3-}$		$[Cr(H_2O)_6]^{3+}$	
		(cm^{-1})	(nm)	(cm^{-1})	(nm)
ν_1	$^4A_{2g} \rightarrow {}^4T_{2g}$	17500	571	17400	575
ν_2	$^4A_{2g} \rightarrow {}^4T_{1g}(F)$	24000	417	24700	405
ν_3	$^4A_{2g} \rightarrow {}^4T_{1g}(P)$	38100	263	37000	270

Three absorption bands (ν_1, ν_2, and ν_3) are also observed in the solid state of all three crystals. The RedCubic shows absorption bands at 263, 421, and 571 nm; RedRhombo at 257, 419, and 567 nm ; Blue at 269, 421, and 579 nm. For comparison, the absorption bands of the dark green $K_3[Cr(C_2O_4)_3].3H_2O$ appear at 258, 420, and 580 nm. All four complexes, RedCubic, RedRhombo, Blue, and $K_3[Cr(C_2O_4)_3].3H_2O$ share the same ligand and the same chromophore Cr^{3+}. The reason they show different colors is due to the Cr^{3+} ions are in slightly different compressed field resemble that

occurred in ruby. The ruby is a gemstone composed of Al_2O_3 with Cr^{3+} impurities. The structure consist of Al^{3+} ion and O^{2-} ion. The crystal lattice was hexagonal closest pack, hcp, of O^{2-} and Al^{3+} inserted in octahedral hole. The $3d^3$ ion replaces Al^{3+} in its approximately octahedral site within the corumdum lattice because of very similar sizes between Cr^{3+} (0.75Å) and Al^{3+} (0.67 Å). Notice that Cr^{3+} is slightly larger than Al^{3+} so the presence of different force field of oxide ligands to Cr^{3+} and Al^{3+}. Chromium ion in this case will be pressed by the smaller ligand framework hence it absorbs at different wavelength causing the ruby color seen by the human eyes as red which is in contrast to the green color when Cr^{3+} is in normal oxide framework, for example, in Cr_2O_3. The absorption spectrum of ruby is shown in Figure 37, two absorption bands at 560 (ν_1) and 410 (ν_2) nm (or 17,800 and 34,400 cm^{-1}) correspond to the yellowish green and blue regions, respectively, therefore, leaving the red region unabsorbed and is seen as the color of ruby. Similarly, in the RedCubic and RedRhombo the ν_1 and ν_2 bands are slightly higher in energy compared to those in $[Cr(C_2O_4)_3]^{3-}$ because the Cr^{3+} ions which replace the Al^{3+} ions are also pressed by the smaller oxalato ligand framework. This results in the wider separation between the $^4A_2$ ground state and $^4T_{1g}(F)$ and $^4T_{1g}(P)$ excited states (Figure 35a). The absorption bands ν_1 and ν_2, therefore, are shifted to the high energy side but only slightly compared with $K_3[Cr(C_2O_4)_3].3H_2O$. The color thus shifts toward red instead of dark green.

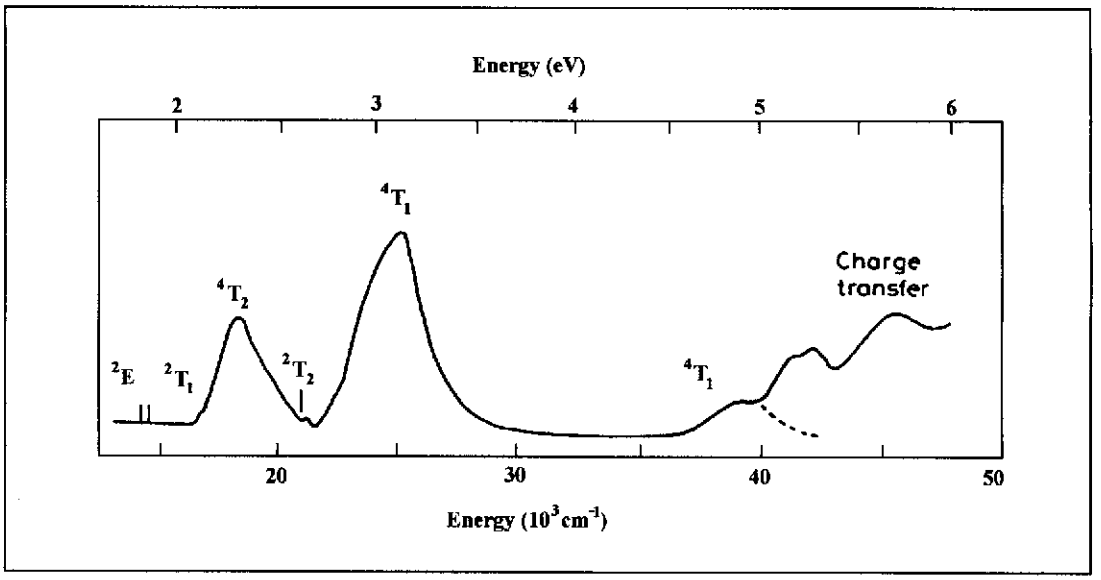

Figure 37 Absorption spectrum of ruby, (Cr^{3+} impurities in corumdum, Al_2O_3). The bands are assigned to transitions from the $^4A_{2g}$ ground state, according the energy levels of Figure 34a (Cox P. A., 1992).

In addition, RedCubic and RedRhombo also show a color change under different light sources which are similar to that observed in the gemstone alexandrite. The alexandrite effect of RedCubic is shown in the Figure 38.

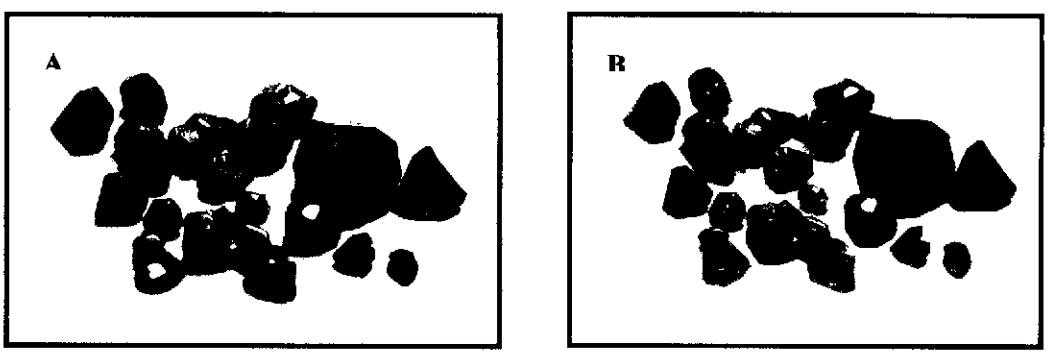

Figure 38 The color-change RedCubic is dark blue in day (or fluorescent) light, A, and reddish violet in incandescent light, B.

One very special feature of ruby is its ability to emit laser. To understand this one must consider Figure 35b in conjunction with Figure 37. Starting from the $^4A_{2g}$ ground state, the spin selection rule ($\Delta S = 0$) shows that only excited quartet states will appear strongly in absorption. This allows the main feature of the spectrum to be assigned as shown in Figure 37. Full energy-level diagram for a $Cr^{3+}(d^3)$ ion in octahedral field is shown in Figure 35b. The ^2G level is important to laser effect. The much weaker spin-forbidden transitions to ^2E_g and $^2T_{2g}$ states can also be seen; these are important in emission, that from the ^2E_g state being used in the ruby laser. Figure 40(top) shows a more detailed view of these spin-forbidden bands, together with part of the emission spectrum produced states have a small splitting, which is a consequence of the true site symmetry of Cr^{3+} being not quite octahedral. Emission from ^2E, known as the 'R' lines, forms the basis of the ruby laser, historically interesting as the first system in which optical laser operation was achieved.

Light with sufficient energy can excited the system from $^4A_{2g}$ ground state to $^4T_{2g}$ and $^4T_{1g}(F)$ excited states. The life time in the excited states ate usually short so promptly after excitation the system must relax or fall back to ground state. The presence of the doublet states $^2T_{1g}$ and ^2E_g near the $^4T_{2g}$ state is the key factor to the laser behaviour of ruby. The relaxation from $^4T_{2g}$ can go to these near by doublet states, instead of going directly to the $^4A_{2g}$ ground state, and remain there considerably longer than the life time of the quartet excited states. Since the excitation and relaxation take place continuously this causes the population at the doublet states ($^2T_{1g}$ and ^2E_g) to increase dramatically. Eventually the over populated doublet states relax to ground state $^4A_{2g}$ resulting in an emission of photo with wavelength 694 nm. Since the population is densed so the high intensity of the emitted light and this is known as the laser light produced by the ruby crystal. This can be shown diagramatically in Figure 39.

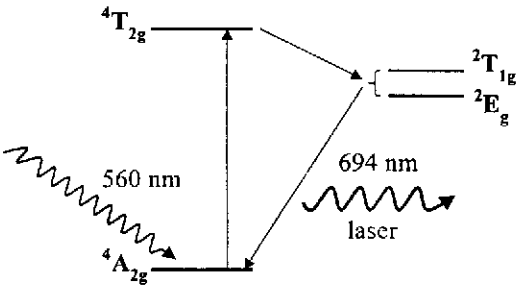

Figure 39 partial energy level diagram of ruby laser

In order to see how this emission occurs, and also to understand the widths of the different transitions, it is necessary to consider the way in which the equilibrium geometry surrounding the Cr^{3+} ion changes in the various electronic states. In Figure 40(bottom) the horizontal coordinate represents a local vibrational mode, leading to an alteration of the Cr-O distance. In the Tanabe-Sugano diagram in Figure 36 the energy of the excited quartet states increases rapidly with the crystal field splitting, Δ; this is understandable as, for example, $^4T_2$ arises from the configuration t^2e^1 where an electron has been excited to the more antibonding *e* orbitals. Thus we expect the equilibrium bond length to increase in this states, as indicated in the figure. On the other hand, the ^2E and $^2T_2$ states are almost horizontal in the Tanabe-Sugano diagram, as they come largely from a rearrangement of electrons within the t_2 levels, and do not involve a change in bonding. Their potential curves are therefore almost directly above that for the $^4A_2$ ground state. The vertical line in Figure 40(bottom) show transition taking place according to the Franck-Condon principle. The transition to $^4T_2$ is accompanied by vibrational excitation, and it is the partly unresolved vibrational structure which broadens the line. On the other hand, very little vibrational excitation should accompany the doublet transitions, which are therefore sharp.

Figure 40(bottom) also shows that the $^4T_2$ surface crosses the doublet ones; thus before direct emission from $^4T_2$ can take place, there is a high probability of non-radiative crossing into the doublets. Most emission in ruby comes from the lower of

these, ^2E. The spectrum shows that there is a vibrational mode at 375 cm^{-1} weakly excited in the ^2E. This appears at higher energy in absorption, as one quantum of this mode is produced in the excited state, but at lower energy in emission, which occurs primarily from the vibrationally relaxed upper level, and leaves one quantum of vibrational in the ground state. The 'mirror-image' form of absorption and emission is quite common in the spectra of localized states.

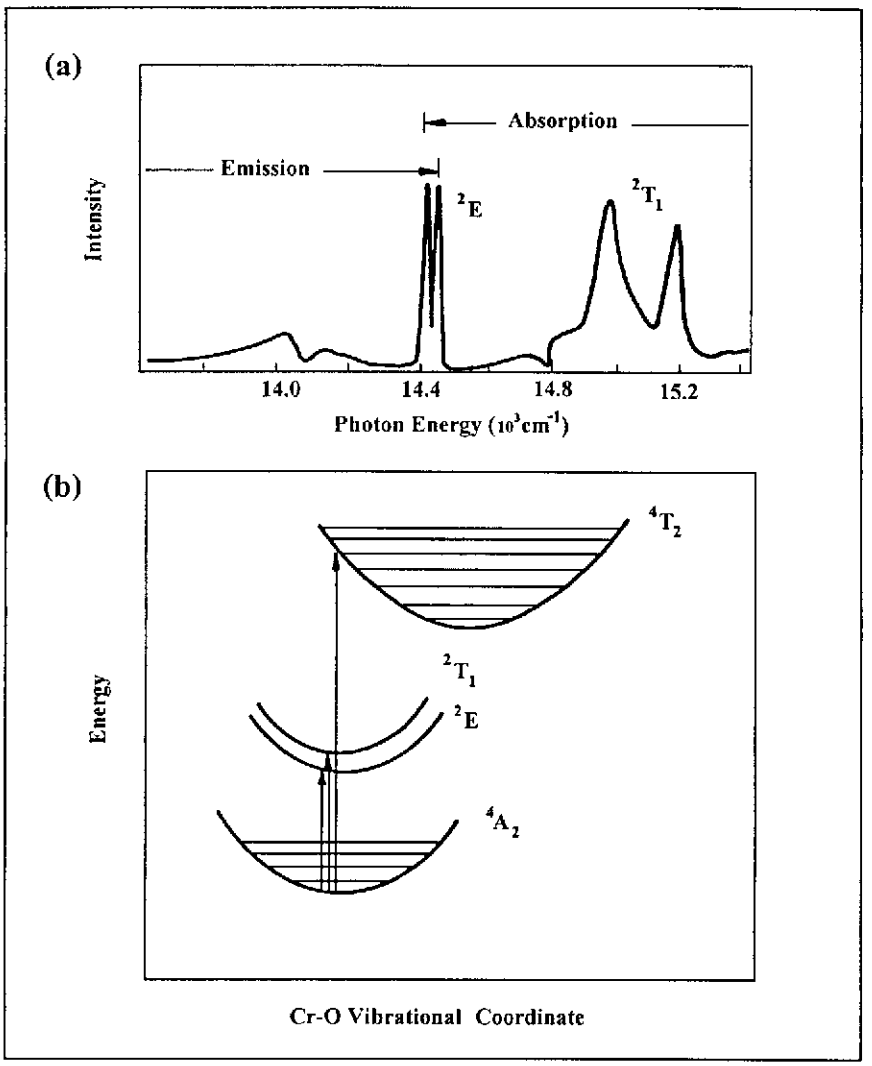

Figure 40 (a) Part of the absorption and emission spectra of ruby (Al_2O_3 with Cr^{3+} impurities), showing the spin-forbidden transitions under high resolution. (b) Potential curves for ground and excited crystal field states for octahedral Cr^{3+} (d^3). The horizontal coordinate represents a local Cr-O stretching mode. Vertical lines show the band maxima for absorption and emission processes, as predicted by the Franck-Condon principle (Cox P. A., 1992).

4.2.6 Infrared spectroscopic technique

Characterization of complexes was mainly based on x-ray diffraction studies. Nevertheless, infrared spectroscopy is a good indicator of incorporation of metal ion and ligands into the complex system. Studies of the effect of coordination on the infrared spectra of metallic complexes afford valuable information on the nature of the metal-ligand bond and the stability of the complex. Coordination usually causes (1) appearance of new bands and splitting of the degenerate modes due to lowering of symmetry, (2) frequency shifts of the bands, and (3) intensification of the spectra. IR spectra were recorded as KBr discs in the region 4000-370 cm^{-1} on Perkin-Elmer Spectrum GX FT-IR spectrometer providing the information of the coordination mode of ligands. It is well known that the $C_2O_4^{2-}$ ligand can coordinate to the metal as a monodentate as well as a bidentate one (Figure 41). Therefore, comparison of the infrared spectra of monodentate and bidentate metallic complexes of this ligand will be of considerable interest.

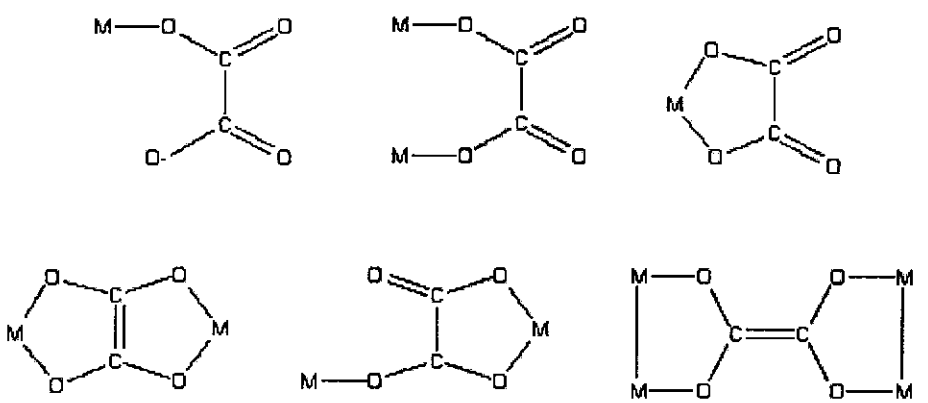

Figure 41 The main linkage types of oxalate ligand with metal (Cotton et al., 1999)

The infrared spectra of oxalato complexes have been studied extensively. Empirical band assignments had been made by using the results of normal coordinate analysis on the free oxalate ion. Free oxalate ion has high symmetry of V_h and exhibits 12 fundamentals (Nakamoto K., 1957). Among those, 9 are in-plane and 3 are out-of-

plane vibrations. The number of infrared active in-plane modes are only 4 in V_h. If the symmetry is reduced to C_{2v} by coordination, all the 9 modes become infrared active. Whereas, Clark et al., 2002 reported the oxalate ion was planar (D_{2h} symmetry) or twisted (D_2 or D_{2d} symmetry). The group theoretical predictions for the Raman activity of the normal modes of the oxalate ion were that there should be 0, 8, and 5 coincidenced for D_{2h}, D_2, and D_{2d} symmetry, respectively. Atomic displacements of oxalate anion are shown in Figure 42.

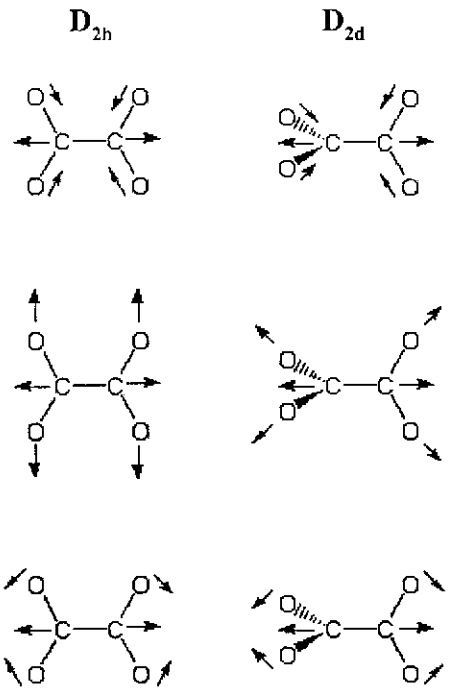

Figure 42 Atomic displacements in the totally symmetric normal modes of the planar and 90° twisted oxalate anion (Clark et al., 2002)

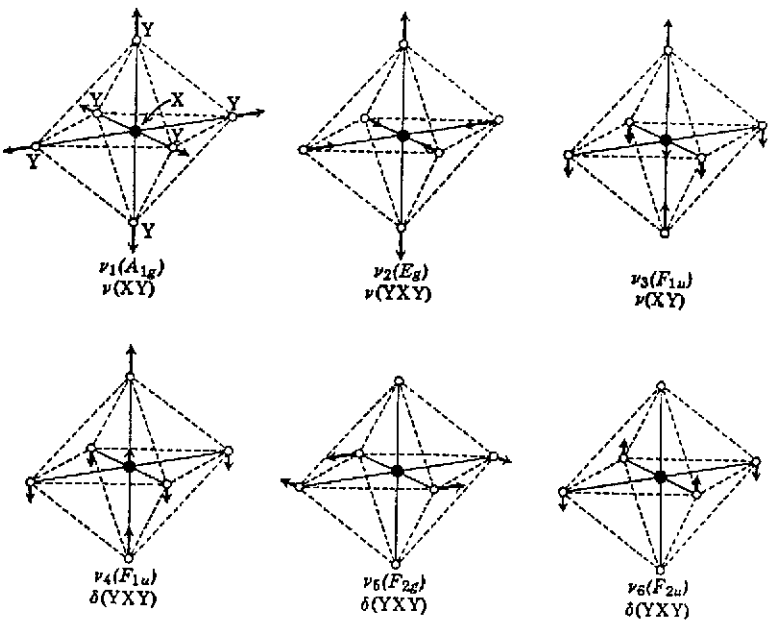

Figure 43 Normal modes of vibration in octahedral XY_6 molecules (Nakamoto K., 1986).

The oxalate complexes were distorted octahedral coordination. It could be explained as octahedral XY_6 molecules. Figure 43 illustrates the six normal modes of vibration of an octahedral XY_6 molecules. Vibrations ν_1, ν_2, and ν_5 are Raman active, whereas only ν_3 and ν_4 are infrared active. Since ν_6 is inactive in both , its frequency is estimated from an analysis of combination and overtone (Nakamoto K., 1986). Fujita et al., 1962 carried out normal coordination analysis on the 1:1 (metal:ligand) model of the $[M(C_2O_4)_2]^{2-}$ and $[M(C_2O_4)_3]^{3-}$ series, and obtained the band assignment listed in Table 15. In the divalent metal series, ν(C=O) (average of ν_1 and ν_7) becomes higher, and ν(C-O) (ν_2 and ν_8) becomes lower, as ν_4 (M-O) becomes higher. These results of Table 15 suggest that, as the M-O bond become stronger, the C-O becomes weaker and the C=O and the C-C bonds becomes stronger. Thus a shift of the ν(M-O) band to higher frequency is expected to accompany a shift

of the ν(C-O) band to a lower frequency, together with a shift of the ν(C=O) band to a higher frequency. According to normal coordination analysis (Fujita et al., 1962) both ν(C-O) and ν(M-O) stretching vibrations are coupled with other modes (see in Table 15). Nevertheless, linear relationships exist between ν_4 (predominantly ν(M-O)) and the average of ν_1 and ν_7 (both are νa(C=O)), and between ν_4 either ν_2 and ν_8 (both are predominantly νs (C-O)). In oxalato complexes of trivalent metals, strict linear relationships between the frequencies do not exist. It is found, however, that ν_4 and ν_{11} (both are predominantly ν(M-O)) increase along the series Fe< V < Cr < Co < Al (Nakamoto K., 1970).

In order to clarify the mode of bonding the IR spectra of the mononuclear fragments $K_3[Cr(C_2O_4)_3]\cdot 3H_2O$ and $K_3[Al(C_2O_4)_3]\cdot 3H_2O$ were compared with the spectra of the RedCubic, RedRhombo, and Blue complexes. Since the IR spectra of all the product complexes are similar, discussion is confined to the most important vibration in the 370-4000 cm^{-1} region in relation to the structure. The most relevant IR absorption bands of the products and the mononuclear complexes $K_3[Cr(C_2O_4)_3]\cdot 3H_2O$ and $K_3[Al(C_2O_4)_3]\cdot 3H_2O$, together with their assignments are given in Table 10 (Chapter 3). It is noteworthy that the spectra of the mononuclear complexes $K_3[Cr(C_2O_4)_3]\cdot 3H_2O$ and $K_3[Al(C_2O_4)_3]\cdot 3H_2O$ only show the typical bidentate coordination mode of the oxalato groups. However, the IR spectra of the three products exhibit bands corresponding to the bidentate oxalato ligand (ca. 1700, 1680, 1650 cm^{-1}) [ν_{as}(CO)]; 780 cm^{-1} [δ(CO)] and also the bridging oxalato ligand (ca. 1620 cm^{-1}) [ν_{as}(CO)]; 1380, 1340 cm^{-1} [ν_s(CO)], suggesting that the oxalato groups of the mononuclear fragments coordinate with inner K(I) ions. They are assignable to the bridging coordination mode of oxalate ligand of lower symmetry, well characterized by the x-ray diffraction study shown in Figure 1 (Chapter 3).

The report of Fujita, et al., 1962 carried out normal coordinate analyses on the 1:3 (metal-ligand) model of the $[M(C_2O_4)_3]^{3-}$ series, M = Cr, Al (Nakamoto et al., 1977) and obtained the band assignments listed in Table 15. The IR data of the synthesized $K_3[Cr(C_2O_4)_3]\cdot 3H_2O$ and $K_3[Al(C_2O_4)_3]\cdot 3H_2O$ complexes are identical to that shown in the report of Nakamoto K., 1978 and Arco et al., 2003. Both of the complexes show intense bands in the range 1700-1600 cm^{-1}, corresponding to C=O stretching. The C—O stretching modes in complexes appear in the regions 1450-1350 and 1300-1200 cm^{-1} and are slightly shifted to lower frequencies, about 20 cm^{-1}, compared to free ligand. This is a good indication of O coordination. The frequencies of the M—O stretching modes occurred in the region 600-400 cm^{-1}. For this work, the synthesized $K_3[Cr(C_2O_4)_3]\cdot 3H_2O$ shows Cr-O stretching modes at 800, 543, and 417 cm^{-1} while Al-O stretching modes at 806, 583, and 495 cm^{-1} in the synthesized $K_3[Al(C_2O_4)_3]\cdot 3H_2O$. This indicated that the O atoms were bonded to the metals center.

The C=O stretching of RedCubic, RedRhombo, and Blue show intense bands in the range 1723-1675 cm^{-1}. Whereas, the C—O stretching modes show intense bands in the range 1408-1271 cm^{-1}. The frequencies of the M—O stretching modes occurred in the region 586-473 cm^{-1} and they show nearly Al-O stretching because they have 97 percent of aluminium (3 percent of chromium) which identical to x-ray result. In addition, all oxalato complexes show bands about 3500 cm^{-1} which arise from OH stretching of water and correspond to x-ray and TGA results.

Table 15 Observed frequencies of various vibrational modes of $K_3[Cr(C_2O_4)_3]\cdot 3H_2O$ and $K_3[Al(C_2O_4)_3]\cdot 3H_2O$ complexes $(cm)^{-1}$(Fujita et al., 1962).

$K_3[Cr(C_2O_4)_3]\cdot 3H_2O$	$K_3[Al(C_2O_4)_3]\cdot 3H_2O$	Assignments	ν
1708	1722	νas(C=O)	ν_7
1684, 1660	1700, 1683	νas(C=O)	ν_1
1387	1405	νs(C-O) + ν(C-C)	ν_2
1253	1292, 1269	νs(C-O) + δ(O-C=O)	ν_8
893	904	νs(C-O) + δ(O-C=O)	ν_3
810, 798	820, 803	δ(O-C=O) + ν(M-O)	ν_9
595	-	Crystal water	-
543	587	ν(M-O) + ν(C-C)	ν_4
485	436	δ(O-C=O) + ring def.	ν_{10}
415	487	ν(M-O) + ring def.	ν_{11}
358	364	δ(O-C=O)	ν_5
313	-	π(out of plane)	-

4.2.7 Thermogravimetry analysis and Differential scanning calorimetry

Oxalate anion is a good ligand and can be coordinated with many transition and non-transition metals. Their thermal decomposition processes are relatively complicated because of the reduction property of $C_2O_4^{2-}$. The thermal decomposition of the type $K_3[M(C_2O_4)_3]\cdot 3H_2O$ (where M = Cr, Al, and Fe) were studied by Jun et al., 2003. Beginning, the thermal decomposition processes of $K_3[Al(C_2O_4)_3]\cdot 3H_2O$ and $K_3[Cr(C_2O_4)_3]\cdot 3H_2O$ were reported by Broadbent et al., 1969 and showed that water was lost above 40°C, the rate increasing up to 100°C and a stable anhydrous complex formed over the range 150 to 375°C. After that the complex broke down to mixture of potassium carbonate, potassium oxide, and alumina. This is summarized in Table 16.

Table 16 $K_3[Al(C_2O_4)_3]\cdot 3H_2O$ x-ray diffraction analysis of residues and compounds in residues (Broadbent et al., 1969)

Heat treatment, $^{\circ}C$	x-ray findings
200 (air)	Hydrated complex
	Anhydrous complex
420 (air)	Complicated pattern includes K_2CO_3,
	$K_2C_2O_4$, and some aluminate ($K_2O.Al_2O_3$)
600 (air)	K_2CO_3 and trace of aluminate
800 (air)	K_2CO_3 and trace of aluminate
1000 (air)	K_2CO_3, strong lines of aluminate
430 (nitrogen)	Complicated pattern similar to that in air
	at 420°C, but no aluminate
900 (air)	K_2CO_3 and trace of aluminate

After that Verdonk A.H., (1971) studied the thermal decomposition path of aluminium oxalate in 5 steps as follows.

$$K_3[Al(C_2O_4)_3].3H_2O \longrightarrow K_3[Al(C_2O_4)_3]_{(s)} + 3H_2O \quad (23\text{-}120^{\circ}C)$$

$$K_3[Al(C_2O_4)_3]_{(s)} \longrightarrow K_2CO_{2\,(s)} + 0.5K_2CO_{3\,(s)} + 0.5Al_2O_{3\,(s)} + 2CO_{(g)} + 1.5CO_{2\,(g)}$$

$$(320\text{-}435^{\circ}C)$$

$$K_2C_2O_{4\,(s)} \longrightarrow K_2CO_{3\,(s)} + CO_{(g)} \quad (435\text{-}475^{\circ}C)$$

$$0.5K_2CO_{3\,(s)} + 0.5Al_2O_{3\,(s)} \longrightarrow KAlO_{2\,(s)} + CO_{2\,(g)} \quad (475^{\circ}C)$$

$$K_2CO_{3\,(s,\,l)} \longrightarrow K_2O_{(s)} + CO_{2\,(g)}$$

The water content can be variable and even "dry" samples are reported as having 3 moles of water by Foster, et al., 1982 that dehydration occurs in 3 steps according to the following reactions.

$K_3[Al(C_2O_4)_3]\cdot 3H_2O_{(s)} \rightarrow K_3[Al(C_2O_4)_3]\cdot 7/3H_2O_{(s)} + 2/3H_2O_{(g)}$ (50-70°C)

$K_3[Al(C_2O_4)_3]\cdot 7/3H_2O_{(s)} \rightarrow K_3[Al(C_2O_4)_3]\cdot 1/3H_2O_{(s)} + 2H_2O_{(g)}$ (80-130°C)

$K_3[Al(C_2O_4)_3]\cdot 1/3H_2O_{(s)} \rightarrow K_3[Al(C_2O_4)_3] + 1/3H_2O_{(g)}$ (130-170°C)

$K_3[Al(C_2O_4)_3]_{(s)} \rightarrow K_3[Al(CO_3)_2O]_{(s)} + 3\ CO_{(g)} + CO_{2(g)}$ (380-480°C)

$2K_3[Al(CO_3)_2O]_{(s)} \rightarrow K_6Al_2(CO_3)_3O_{3(s)} + CO_{2(g)}$ (490-525°C)

This agreed with the work of Haines P. J., (1999) where he reported that the thermal analysis of $K_3[Al(C_2O_4)_3]\cdot 3H_2O$ showed more complicated situations than might be expected. Firstly, the water content was reported as having 3 moles of water. Secondly, hydroxo-oxalato aluminates might be present as a contaminant. The sample used in this investigation was analysed by ICP and found to contain 25.8% K (theory: 25.3%) and 5.6%Al (theory: 5.8%). It also appeared to pick up moisture easily and contained slightly more than $3H_2O$. The DSC showed several dehydration endotherms between room temperature and 300°C, with the largest one occurred around 100°C. This was confirmed by TG and was similar to the reported behavior of the loss of adherent water followed by a series of poorly-resolved dehydration steps at increasing temperature. It corresponded to the report of Broadbent et al., 1969.

$K_3[Al(C_2O_4)_3]\cdot nH_2O \rightarrow K_3[Al(C_2O_4)_3] + nH_2O$ (40-100°C)

$2K_3[Al(C_2O_4)_3] \rightarrow 3K_2C_2O_4 + Al_2O_3 + 3CO + 3CO_2$ (400-500°C)

$K_2C_2O_4 \rightarrow K_2CO_3 + CO$

These steps was followed at higher temperatures by reaction to form the aluminate: $K_2CO_3 + Al_2O_3 \rightarrow K_2Al_2O_4 + CO_2$ and also the formation of K_2O. This accounted for the further mass losses up to 1300°C.

The thermal analysis of $K_3[Cr(C_2O_4)_3]\cdot 3H_2O$ showed that it lost water around 100°C and the anhydrous complex oxalate started to decompose, possibly accompanied by a phase change, around 300°C, and the decompositions of the oxalates occurred over the range 300-500°C and were followed in the later stages and at higher temperatures by the reaction in air to form the yellow potassium chromate K_2CrO_4(Haines P. L., 1999).

$$K_3[Cr(C_2O_4)_3]\cdot 3H_2O \longrightarrow K_3[Cr(C_2O_4)_3] + 3H_2O \quad (100^{\circ}C)$$

$$K_3[Cr(C_2O_4)_3] \longrightarrow 3/2K_2CO_3 + 1/2Cr_2O_3 + 3CO + 3/2CO_2 \quad (300\text{-}500^{\circ}C)$$

$$K_2CO_3 + 1/2Cr_2O_3 + 3/4O_2 \longrightarrow K_2CrO_4 + CO_2$$

Whereas, House et al., 1980 reported that the same decomposition took place in 5 steps according to equations

$$K_3[Cr(C_2O_4)_3]\cdot 3H_2O_{(s)} \longrightarrow K_3[Cr(C_2O_4)_3]_{(s)} + 3H_2O_{(g)} \quad (100\text{-}165^{\circ}C)$$

$$K_3[Cr(C_2O_4)_3]_{(s)} \longrightarrow K_3[Cr(C_2O_4)_{3/2}(CO_3)_{3/2}]_{(s)} + 3/2CO_{(g)} \quad (185\text{-}265^{\circ}C)$$

$$K_3[Cr(C_2O_4)_{3/2}(CO_3)_{3/2}]_{(s)} \longrightarrow K_3[Cr(C_2O_4)_{1/2}(CO_3)_{5/2}]_{(s)} + CO_{(g)} \quad (285\text{-}310^{\circ}C)$$

$$K_3[Cr(C_2O_4)_{1/2}(CO_3)_{5/2}]_{(s)} \longrightarrow K_3[Cr(CO_3)(O)_2]_{(s)} + 1/2CO_{(g)} + 2CO_{2(g)} \quad (345\text{-}485^{\circ}C)$$

$$K_3[Cr(CO_3)(O)_2]_{(s)} \longrightarrow K_3CrO_{3(s)} + CO_{2(g)}$$

Moreover, Arco et al., (2003) reported decomposition of $K_3[Cr(C_2O_4)_3]\cdot 3H_2O$ that the first weight loss, with a corresponding endothermic peak at 105°C, was due to removal of crystallization water; the main weight loss was composed of two consecutive processes, giving rise to an exothermic peak at 381°C, immediately followed by a weaker shoulder at 441°C. The phases identified by PXRD after these processes were K_2CrO_4 and $K_2C_2O_4$; this last decomposes to K_2CO_3, whose melting

was responsible for the sharp endothermic peak (without weight loss) at 894°C without the reactions.

Finally, Jun L., (2003) studied the thermal decomposition processes of the complexes of $K_3[Al(C_2O_4)_3]\cdot 3H_2O$ and $K_3[Cr(C_2O_4)_3]\cdot 3H_2O$ which occurred according to the reactions.

Steps	$K_3[Al(C_2O_4)_3]\cdot 3H_2O$	$K_3[Cr(C_2O_4)_3]\cdot 3H_2O$
I	$\downarrow -3H_2O$ (30-150°C)	$\downarrow -3H_2O$ (30-150°C)
	$K_3[Al(C_2O_4)_3]$	$K_3[Cr(C_2O_4)_3]$
II	$\downarrow -1/2(3CO_2 + 6CO)$ (350-500°C)	$\downarrow -1/10(16CO + 9CO_2)$ (350-450°C)
	$1/2Al_2O_3 + 3/2K_2CO_3$	$3/2K_2C_2O_4 + 1/5(Cr_3O_4) + Cr_2(CO_3)_3$
III	-	$\downarrow -1/3(37CO + 23CO_2)$ (450-500°C)
		$3/2K_2CO_3 + 1/3Cr_3O_4$

In this work, the decomposition of oxalato complexes were studied and the amount of water molecule were identified by percentage of weight loss. Synthesized $K_3[Al(C_2O_4)_3]\cdot 3H_2O$ and $K_3[Cr(C_2O_4)_3]\cdot 3H_2O$ were found to lose $3H_2O$. It corresponded to TGA result. That is $K_3[Al(C_2O_4)_3]\cdot 3H_2O$ lost 10.38% of weight (theory: 11.69%) in the range from room temperature to 100°C. The DSC showed endothermic peak at 94°C. $K_3[Cr(C_2O_4)_3]\cdot 3H_2O$ lost 10.96% of weight (theory: 11.09%) in the range room from temperature to 180°C. The DSC showed endothermic peak at 113°C.

For the three products in this work (RedCubic, RedRhombo, and Blue) only the structure of RedRhombo could be solved by the x-ray crystallographic method as $K_{18}\{K[Al_{0.97}Cr_{0.03}(C_2O_4)_3]_6\}Cl.18H_2O$. It has 18 molecules of water. The TGA lost 11.08% of weight (theory: 11.35%) in the range from room temperature to 182°C and

DSC showed endothermic peak at 102°C. It lost rapidly 28.64% of weight at 182-200°C because of K-O bond were broken and then it showed decomposition spectrum similar to $K_3[Al(C_2O_4)_3]\cdot 3H_2O$ at higher temperature.

The structure of RedCubic and Blue could not be solved. But TGA of RedCubic lost 16.10% of weight in the range from room temperature to 200°C and DSC showed endothermic peak at 101, 125, and 135°C whereas, TGA of the Blue lost 10.15% of weight in the range from room temperature to 100°C and DSC showed endothermic peak at 91°C. Both have crystal water but the RedCubic has percentage of water more than the Blue. The structure of RedCubic was different from the two starting complexes. The fact that the Blue lost 10.15% of weight which were similar to the percentage loss of $K_3[Al(C_2O_4)_3]\cdot 3H_2O$ and $K_3[Cr(C_2O_4)_3]\cdot 3H_2O$ led to the conclusion that they might have similar structures. This conclusion is supported by the powder x-ray data showing that they all belong to the same space group $P2_1/c$.

By the follow of the experimental results that three types of crystals were obtained, two with dark red color almost black and the other with blue color. They are designed as RedCubic, RedRhombo, and Blue. The structure of RedCubic and Blue could not be solved while RedRhombo could be solved as $K_{18}\{K[Al_{0.97}Cr_{0.03}(C_2O_4)_3]_6\}Cl.18H_2O$. The crystal system of RedCubic is cubic. RedRhombo is rhombohedral with space group $R\bar{3}$ while Blue is monoclinic with space group $P2_1/c$ similar to the starting compounds ($K_3[Al(C_2O_4)_3].3H_2O$ and $K_3[Cr(C_2O_4)_3].3H_2O$). The three complexes were readily soluble in water. They shows absorption peaks of chromium at 420 and 572 nm and shows M-O stretching in the region 600-400 cm^{-1}. They have two metal, aluminium and chromium, in the complex and oxalate was ligand. The small amount of chromium presents in the products is similar to corundum and shows alexandrite effect.